Research Article | Vol. 26, No. 10 | 14 May 2018 | OPTICS EXPRESS 12723
Optics EXPRESS

Simplified physical modeling of parallel-aligned liquid crystal devices at highly non-linear tilt angle profiles

JORGE FRANCÉS,[1,2] ANDRÉS MÁRQUEZ,[1,2,*] FRANCISCO J. MARTÍNEZ-GUARDIOLA,[1,2] SERGIO BLEDA,[1,2] SERGI GALLEGO,[1,2] CRISTIAN NEIPP,[1,2] INMACULADA PASCUAL,[1,2] AND AUGUSTO BELÉNDEZ,[1,2]

[1]*Dept. de Física, Ing. de Sistemas y Teoría de la Señal, U. de Alicante, Ap. 99, E-03080, Alicante, Spain*
[2]*I.U. Física Aplicada a las Ciencias y las Tecnologías U. de Alicante, Ap. 99, E-03080, Alicante, Spain*
[3]*Dept. de Óptica, Farmacología y Anatomía, Universidad de Alicante, Ap. 99, E-03080, Alicante, Spain*
[*]*andres.marquez@ua.es*

Abstract: In recent works, we demonstrated the accuracy and physical relevance of a highly simplified reverse-engineering analytical model for a parallel-aligned liquid crystal on silicon devices (PA-LCoS). Both experimental measurements and computational simulations applying the rigorous split-field finite difference time domain (SF-FDTD) technique led to this conclusion in the low applied voltages range. In this paper, we develop a complete rigorous validation covering the full range of possible applied voltages, including highly non-linear liquid crystal (LC) tilt angle profiles. We demonstrate the applicability of the model for spectral and angular retardation calculations, of interest in spatial light modulation applications. We also show that our analytical model enables the calculation of the retardance for novel PA-LC devices as a function of the LC compound and cell gap, becoming an appealing alternative to the usual numerical approaches for PA-LC devices design.

OCIS codes: (050.1755) Computational electromagnetic methods; (160.3710) Liquid crystals; (230.3720) Liquid-crystal devices; (230.6120) Spatial light modulators; (230.2090) Electro-optical devices; (260.1440) Birefringence.

References and links

1. P. Yeh and C. Gu, *Optics of Liquid Crystal Displays* (John Wiley & Sons Inc, 1999).
2. S. T. Wu and D. K. Yang, *Reflective Liquid Crystal Displays* (John Wiley & Sons Inc, 2005).
3. V. G. Chigrinov, *Liquid Crystal Devices: Physics and Applications* (Artech House, 1999).
4. N. Collings, T. Davey, J. Christmas, D. Chu, and B. Crossland, "The Applications and Technology of Phase-Only Liquid Crystal on Silicon Devices," J. Disp. Technol. **7**(3), 112–119 (2011).
5. Z. Zhang, Z. You, and D. Chu, "Fundamentals of phase-only liquid crystal on silicon (LCOS) devices," Light Sci. Appl. **3**(10), 1–10 (2014).
6. G. Lazarev, A. Hermerschmidt, S. Krüger, and S. Osten, "LCOS spatial light modulators: trends and applications," in *Optical Imaging and Metrology: Advanced Technologies*, W. Osten and N. Reingand, eds. (John Wiley & Sons Inc, 2012).
7. A. Hermerschmidt, S. Osten, S. Krüger, and T. Blümel, "Wave front generation using a phase-only modulating liquid-crystal based micro-display with HDTV resolution," Proc. SPIE **6584**, 65840E (2007).
8. A. Lizana, I. Moreno, A. Márquez, E. Also, C. Iemmi, J. Campos, and M. J. Yzuel, "Influence of the temporal fluctuations phenomena on the ECB LCoS performance," Proc. SPIE **7442**, 74420G (2009).
9. J. García-Márquez, V. López, A. González-Vega, and E. Noé, "Flicker minimization in an LCoS spatial light Modulator," Opt. Express **20**(8), 8431–8441 (2012).
10. M. Wang, L. Zong, L. Mao, A. Marquez, Y. Ye, H. Zhao, and F. J. Vaquero, "LCoS SLM Study and Its Application in Wavelength Selective Switch," Photonics **4**(22), 1–16 (2017).
11. F. J. Martínez, A. Márquez, S. Gallego, J. Francés, I. Pascual, and A. Beléndez, "Retardance and flicker modeling and characterization of electro-optic linear retarders by averaged Stokes polarimetry," Opt. Lett. **39**(4), 1011–1014 (2014).
12. F. J. Martínez, A. Márquez, S. Gallego, M. Ortuño, J. Francés, I. Pascual, and A. Beléndez, "Predictive capability of average Stokes polarimetry for simulation of phase multilevel elements onto LCoS devices," Appl. Opt. **54**(6), 1379–1386 (2015).
13. F. J. Martínez, R. Fernández, A. Márquez, S. Gallego, M. L. Álvarez, I. Pascual, and A. Beléndez, "Exploring binary and ternary modulations on a PA-LCoS device for holographic data storage in a PVA/AA photopolymer," Opt. Express **23**(16), 20459–20479 (2015).

#322622 https://doi.org/10.1364/OE.26.012723
Journal © 2018 Received 5 Mar 2018; revised 9 Apr 2018; accepted 12 Apr 2018; published 3 May 2018

Optics EXPRESS

14. F. J. Martínez, A. Márquez, S. Gallego, J. Francés, I. Pascual, and A. Beléndez, "Effective angular and wavelength modelling of parallel aligned liquid crystal devices," Opt. Lasers Eng. **74**, 114–121 (2015).
15. V. G. Chigrinov, H. S. Kwok, D. A. Yakovlev, G. V. Simonenko, and V. I. Tsoy, "LCD Optimization and Modeling," in *SID 04 DIGEST* (2014), pp. 982–985.
16. A. Márquez, J. Francés, F. J. Martínez-Guardiola, S. Gallego, M. L. Álvarez, E. M. Calzado, I. Pascual, and A. Beléndez, "SF-FDTD analysis of a predictive physical model for parallel aligned liquid crystal devices," Proc. SPIE **10395**, 1039509 (2017).
17. A. Márquez, J. Francés, F. J. Martínez-Guardiola, S. Gallego, M. L. Álvarez, E. M. Calzado, I. Pascual, and A. Beléndez, "Computational SF-FDTD evaluation of simplified tilt-angle models for parallel aligned liquid crystal devices," Opt. Eng. **57**, 037110 (2018).
18. I. Abdulhalim and D. Menashe, "Approximate analytic solutions for the director profile of homogeneously aligned nematic liquid crystals," Liq. Cryst. **37**(2), 233–239 (2010).
19. C. Oh and M. J. Escuti, "Time-domain analysis of periodic anisotropic media at oblique incidence: an efficient FDTD implementation," Opt. Express **14**(24), 11870–11884 (2006).
20. M. N. Miskiewicz, P. T. Bowen, and M. J. Escuti, "Efficient 3D FDTD analysis of arbitrary birefringent and dichroic media with obliquely incident sources," Proc. SPIE **8255**, 82550W (2012).
21. A. Taflove and S. C. Hagness, *Computational Electrodynamics: The Finite-Difference Time-Domain Method* (Artech House, 2000).
22. J. Francés, S. Bleda, M. L. Lázara, F. J. Martínez, A. Márquez, C. Neipp, and A. Beléndez, "Acceleration of split-field finite difference time-domain method for anisotropic media by means of graphics processing unit computing," Opt. Eng. **53**(1), 011005 (2013).
23. J. Francés, J. Tervo, S. Gallego, S. Bleda, C. Neipp, and A. Márquez, "Split-field finite-difference time-domain method for second-harmonic generation in two-dimensionally periodic structures," J. Opt. Soc. Am. B **32**(4), 664–669 (2015).
24. J. Li, C.-H. Wen, S. Gauza, R. Lu, and S.-T. Wu, "Refractive Indices of Liquid Crystals for Display Applications," J. Disp. Technol. **1**(1), 51–61 (2005).
25. F. Abeles, *Optics of Thin Films in Advanced Optical Techniques* (North-Holland Publishing Co, 1967).
26. W. H. Southwell, "Gradient-index antireflection coatings," Opt. Lett. **8**(11), 584–586 (1983).
27. A. Márquez, I. Moreno, J. Campos, and M. J. Yzuel, "Analysis of Fabry–Perot interference effects on the modulation properties of liquid crystal displays," Opt. Commun. **265**(1), 84–94 (2006).
28. J. L. Martínez, I. Moreno, M. del Mar Sánchez-López, A. Vargas, and P. García-Martínez, "Analysis of multiple internal reflections in a parallel aligned liquid crystal on silicon SLM," Opt. Express **22**(21), 25866–25879 (2014).
29. A. Lizana, N. Martín, M. Estapé, E. Fernández, I. Moreno, A. Márquez, C. Iemmi, J. Campos, and M. J. Yzuel, "Influence of the incident angle in the performance of Liquid Crystal on Silicon displays," Opt. Express **17**(10), 8491–8505 (2009).
30. F. J. Martínez, A. Márquez, S. Gallego, M. Ortuño, J. Francés, A. Beléndez, and I. Pascual, "Averaged Stokes polarimetry applied to evaluate retardance and flicker in PA-LCoS devices," Opt. Express **22**(12), 15064–15074 (2014).
31. A. Lien, "Extended Jones matrix representation for the twisted nematic liquid-crystal display at oblique incidence," Appl. Phys. Lett. **57**(26), 2767–2769 (1990).
32. I. Moreno, J. V. Carrión, J. L. Martínez, P. García-Martínez, M. M. Sánchez-López, and J. Campos, "Optical retarder system with programmable spectral retardance," Opt. Lett. **39**(19), 5483–5486 (2014).
33. T. G. Brown and Q. Zhan, "Focus Issue: Unconventional Polarization States of Light," Opt. Express **18**, 10775–10776 (2010).
34. X. Zheng, A. Lizana, A. Peinado, C. Ramírez, J. L. Martínez, A. Márquez, I. Moreno, and J. Campos, "Compact LCOS-SLM based polarization pattern beam generator," J. Lightwave Technol. **33**(10), 2047–2055 (2015).

1. Introduction

Widespread use of electrically tunable liquid crystal (LC) devices is a constant in many areas in optics and photonics. Initially developed for intensity transmission modulation in display applications [1,2], they are nowadays very common in a very wide range of non-display applications [3], enabling amplitude, phase or state of polarization modulation. A very appealing LC cell geometry for non-display applications is the parallel-aligned liquid crystal (PA-LC) device since it enables the more energetic efficient phase-only operation without amplitude coupling [4,5]. Parallel-aligned geometry is used in many of the liquid crystal on silicon (LCoS) displays, which are pixelated devices with millions of pixels, widely used as spatial light modulator (SLM) [6], and one of the more technologically advanced liquid crystal devices.

In principle, parallel-aligned geometry is simple to analyze since it is equivalent to a linear variable retarder, therefore its calibration is based on the measurement of only one

Optics EXPRESS

parameter: its linear retardance. However, tunable devices exhibit a series of degradation effects, such as flicker, due to the time variations in the electrical signal addressing as found in LCoS displays [7–9]. Cross-talk effects are also a possibility, especially in pixelated devices where the pixel pitch to thickness ratio of the LC cell decreases, as it is the case in novel LCoS devices with pixel pitch smaller than 8 μm [10]. With these degradation effects in mind, we demonstrated a novel method based on time-average Stokes polarimetry [11], able to provide robust and precise measurement of the linear retardance value even in the presence of flicker. The acquisition of these precise linear retardance measurements is an important step to optimize the performance of the PA-LC devices for applications, such as in diffractive optics [12] or holographic data storage [13]. Additionally, reliable measurements facilitate precise reverse-engineering calibration of the parameters in semi-physical models, directly connected to the inner properties of the LC material and the cell. Recently, we demonstrated a semi-physical model for PA-LCoS devices [14] able to provide the retardance for a very wide range of incidence angles and any wavelength in the visible. The proposed simplified model is based on only three physical parameters whose values are obtained without ambiguities by fitting a limited amount of calibration measurements. These parameters are directly related with the birefringence, cell gap and director profile.

When applying the experimental retardance measurements we do not have any knowledge of the internal properties of the device, since the manufacturer does usually not disclose them. However, to test if a semi-physical model is providing physically meaningful values for its parameters we need to know these internal properties. A non-exhaustive list [1–3] comprises the ordinary and extraordinary refractive indices, cell gap, pre-tilt angle, index of refraction of the glass window, viscosity and elastic coefficients, electrode structure, among others. An alternative yet rigorous approach must be followed. What we actually need is a computational procedure to generate realistic retardance measurements, to be used as the experimental input in the fitting procedure for our semi-physical model. In general, the simulation of the performance of LC devices is divided in two steps. In a first step, accurate calculation of the actual orientation of the LC director across the LC layer as a function of applied voltage is performed by minimizing the total free-energy of the LC cell [1–3]. In a second step, precise numerical methods are used to calculate the electromagnetic propagation of radiation across the cell. This is the procedure followed by commercial packages [15] used by LC device designers and manufacturers. We partially considered such a computational procedure in recent publications [16,17], where we have evaluated the physical significance of the parameters in the model. We approximated the first step, calculation of the LC director profile across the LC layer, using sine-like analytical expressions. This is a reasonable approximation to the realistic non-homogeneous voltage dependent tilt angle profiles [1,18], easy to apply and whose accuracy is good enough as long as the applied voltage is not very large. For the second step, we used the Split-Field Finite Difference Time Domain (SF-FDTD) technique [19,20]. This is an efficient variation of the general FDTD [21], which is a rigorous electromagnetic approach for calculation of light-matter interaction, applied in many areas of Electromagnetism and recently also in Photonics in anisotropic media [19,22]. The Split-Field version economizes in memory resources, thus enabling the increase in the spatial and time resolution of the discrete grid describing the device under test. We have used SF-FDTD in various problems in Photonics [22,23]. However, both in our previous paper [17] and in this work, it is the first time that SF-FDTD is being applied to PA-LC devices for phase-shift and retardance calculations and under oblique incidence.

In contrast with the previous paper [17], now we want to generate the realistic retardance measurements without any limitation on the degree of non-linearity of the voltage dependent tilt angle profiles. We will consider the values for the physical parameters of the well-known E7 LC-compound found in the literature [24] and a cell gap of 2 μm, which is within the range of actual PA-LCoS devices. Once we have generated the LC-director orientation profiles, then we use the SF-FDTD technique to calculate the realistic retardance

Optics EXPRESS

measurements. This enables a rigorous validation of the proposed simplified model considering highly non-linear tilt angle profiles as well. This is also useful to show the range of validity of the sine-like profiles previously used [17]. In this work we further demonstrate the versatility and applicability of the model for spectral and angular retardation calculations, and also as a means to simulate the retardance for novel PA-LC devices as a function of the LC compound and cell gap. These applications make our proposed simplified model an analytical alternative to the usual numerical approaches.

In the next Section we introduce the proposed simplified model for PA-LC devices, and also the details dealing with the construction of the virtual PA-LC cell together with the SF-FDTD computed retardance results. In Section 3, we apply the simplified model to fit the SF-FDTD experimental measurements to obtain the values for the parameters, whose physical relevance is demonstrated. We also demonstrate an efficient approach to calculate the sine-like equivalent tilt profile as a function of the applied voltage. This approach is then applied to the experimental data that we measured in [14]. In Section 4 we use the model for spectral and angular retardation calculations. We further show the potential of the model to simulate the retardance as a function of the LC compound and cell gap. We believe that this is a very important result in the paper. It shows that this is not only a reverse-engineering model but it also constitutes an analytical alternative to the usual numerical approaches for PA-LC devices design and construction. Eventually, in Section 5 we expose the main conclusions.

2. Simplified model and SF-FDTD experiment

2.1. Proposed simplified model

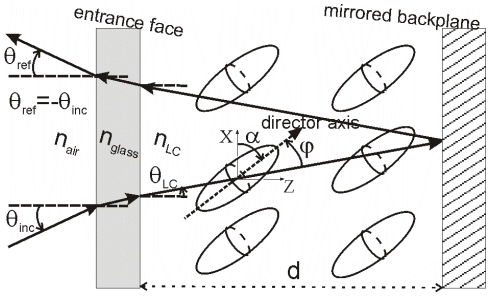

Fig. 1. Diagram for the PA-LC cell considered in the model proposed.

Next we introduce our proposed simplified model for PA-LC devices, whose agreement with experimental measurements was already verified for a commercial reflective PA-LCoS device [14]. In Fig. 1 we show its general diagram for a reflective cell with a cell gap d. Incidence plane and LC director are along the XZ plane. LC molecules have their director axis (optical axis) aligned at an angle ϕ with respect to the traversing light beam direction. θ_{LC} is the refraction angle in the LC medium. The director axis tilts an angle α with respect to the entrance face as a function of the applied voltage V. This is the only voltage dependent magnitude, i.e. $\alpha(V)$. At the backplane the light beam is reflected and a second passage is produced across the LC layer whose effect is equivalent to a forward propagation at an angle $-\theta_{inc}$. In the model we define two off-state parameters, combination of the LC indices ordinary and extraordinary, n_o and n_e, together with the cell gap d. They are $OPL = dn_o$ and $OPD = d\Delta n$, which correspond respectively to the magnitudes of the optical path length for the ordinary component and the optical path difference between extraordinary and ordinary components. Proper derivation leads to the following analytical expression for retardance [14]:

Optics EXPRESS

$$\Gamma = \frac{2\pi}{\lambda}\frac{OPL}{\cos\theta_{LC}}\left[\frac{1+(OPD/OPL)}{1+(OPD/OPL)\cos^2\phi}-1\right]. \quad (1)$$

According to Fig. 1, angle ϕ is given by

$$\phi(\theta_{inc},V) = \frac{\pi}{2}+\alpha(V)\mp\theta_{LC}(\theta_{inc}), \quad (2)$$

where the minus (plus) sign applies for the forward (backward) passage. The total retardance in the PA-LCoS is given by the addition of the forward and backward retardances. In the case of normal incidence and LC director axis parallel to the entrance face, then Eq. (1) simplifies into the well-known expression $\Gamma = 2\pi d\Delta n/\lambda$. Our model produces a much simpler expression and reduces the number of parameters when compared with the exact expressions for a homogeneous uniaxial anisotropic plate, as we demonstrated with experimental data [14].

The voltage dependent tilt angle $\alpha(V)$ does not depend on the wavelength. However, OPD and OPL values depend on the illumination wavelength considered. Once they are fitted at the specific wavelengths used in the experiments for calibration, then we can interpolate them at other wavelengths. The extended Cauchy relation provides a good fit for OPD [14] whereas for OPL values we have to use the basic linear interpolation. As a whole, we are able to obtain the retardance not only for a wide range of incidences (until 45°) but also across the wavelengths in the visible region of the spectrum.

2.2. Nonlinear tilt angle profiles and SF-FDTD computational experiment

In order to produce realistic retardance measurements we consider a PA-LC cell with a cell gap of 2 μm and filled with the nematic LC E7 at room temperature (20°C). The LC mixture E7 is one of the classical compounds found in the literature dealing with LC devices [1]. In contrast with the previous paper [17], where we applied the sine-like analytical profile, now we want to generate the realistic retardance measurements without any limitation on the degree of non-linearity of the voltage dependent tilt angle profiles.

Table 1. Values for the parameters used to simulate the performance of the PA-LC cell.

λ (nm)	n_e	n_o	$\varepsilon_{\parallel}$	$\varepsilon_{\perp}$	k_1(pN)	k_2(pN)	k_3(pN)	d(μm)
633	1.7371	1.5189	19.6	5.1	12	9	19.5	2
532	1.7646	1.5289						
473	1.7935	1.5384						

In Table 1 we summarize the values of the different physical parameters that are necessary to simulate the performance of the LC cell. They are the ordinary n_o and the extraordinary n_e refractive index as a function of the wavelength, the dielectric constants parallel $\varepsilon_{\parallel}$ and perpendicular $\varepsilon_{\perp}$ to the optical axis, the splay k_1, twist k_2 and bend k_3 elastic constants and the cell gap. For the refractive indices we use the tabulated values provided in the paper by Li et al. [24] and interpolate them using the Cauchy relation to produce additional values at other wavelengths. In Table 1 we show specifically the values for the ordinary and the extraordinary refractive index at wavelengths 633, 532 and 473 nm, which are the ones selected to compare with the results provided by the simplified model. However, actually we calculate the retardance of the PA-LC cell across the whole visible spectrum for 18 different equidistant wavelengths running from 473 to 634 nm, as we show below.

To generate the LC-director tilt profiles as a function of the applied voltage we consider the case of strong anchoring [1], which describes very closely the situation found in LCoS devices. This means that LC molecules near the front and rear surfaces of the LC layer are highly attracted by the alignment layer and do not reorient with the applied electric field. The

Optics EXPRESS

general procedure to calculate the profiles can be found for example in Appendix B by Yeh and Gu [1]. In Fig. 2 we show the LC director profiles as a function of the normalized thickness resulting from this calculation for a small subset (indicated in the legend) of the 61 different applied voltages considered. We clearly appreciate how the LC layers next to the surfaces are not free to tilt and the largest tilt is produced in the midlayer. We also note that for voltages smaller than 3 Volts the curves are smooth and with a sine-like shape. For higher voltages then they tend to a saturation plateau.

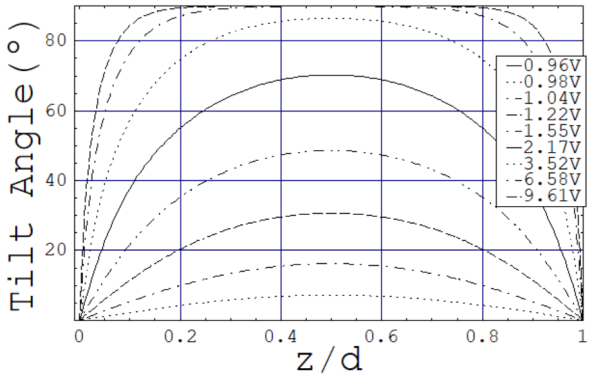

Fig. 2. LC director tilt angle profiles across the thickness of the cell and for various voltages.

Once we generate the LC director profiles, then we apply the SF-FDTD to simulate the propagation of the incident electromagnetic field across the PA-LC cell, following the scheme that we recently presented [17]. The LC cell is composed of the LC layer with a perfectly conducting mirror at the rear surface. The glass window at the entrance is not necessary to be considered, as we discussed in [17]. To the entrance interface air-LC layer we add an antireflection (AR) thin film structure for the visible spectrum [25,26], mimicking the usual AR coating found in PA-LCoS devices. Results with no AR coating have also been produced but are not shown in the paper: the effect of the multiple interferences was very noticeable and were not representative of the experimental results obtained with usual LCoS devices [14] even though in some cases it might be important or even interesting [27,28].

In Fig. 3 we plot the retardance measurements obtained in the simulated experiment and for 4 of the 5 incidence angles: since results for normal and 3° incidences are basically equal, we only show the ones for the latter. The retardance values are presented in a two dimensional contour plot, where the vertical and horizontal axis correspond respectively to the wavelength and the applied voltage. If we do a vertical cut (fixed voltage) we see that retardance decreases with the increase in wavelength, even though some small amplitude oscillations arise at lower voltages. These oscillations are probably due to residual multiple beam interference effects not fully eliminated by the AR coating. If we do a horizontal cut (fixed wavelength) we see the monotonous decrease in retardance as the voltage increases.

From the whole set of wavelengths we chose to analyze the results for the 633, 532 and 473 nm, which sample the visible spectrum in the red, green and blue regions. In Figs. 4(a)-4(c) we show these retardances as a function of voltage respectively for the commented red, green and blue wavelengths. In each of the figures we overlap the curves for the various incidence angles. We clearly appreciate the non-linear monotonous decrease of retardance with voltage. The threshold voltage is about 0.9 V below which LC molecules do not tilt. This is within the typical values in the literature [24]. It is also noticeable that the retardance dynamic range becomes shorter for larger angles of incidence, which was also found in the experimental measurements in previous papers [29,30].

Optics EXPRESS

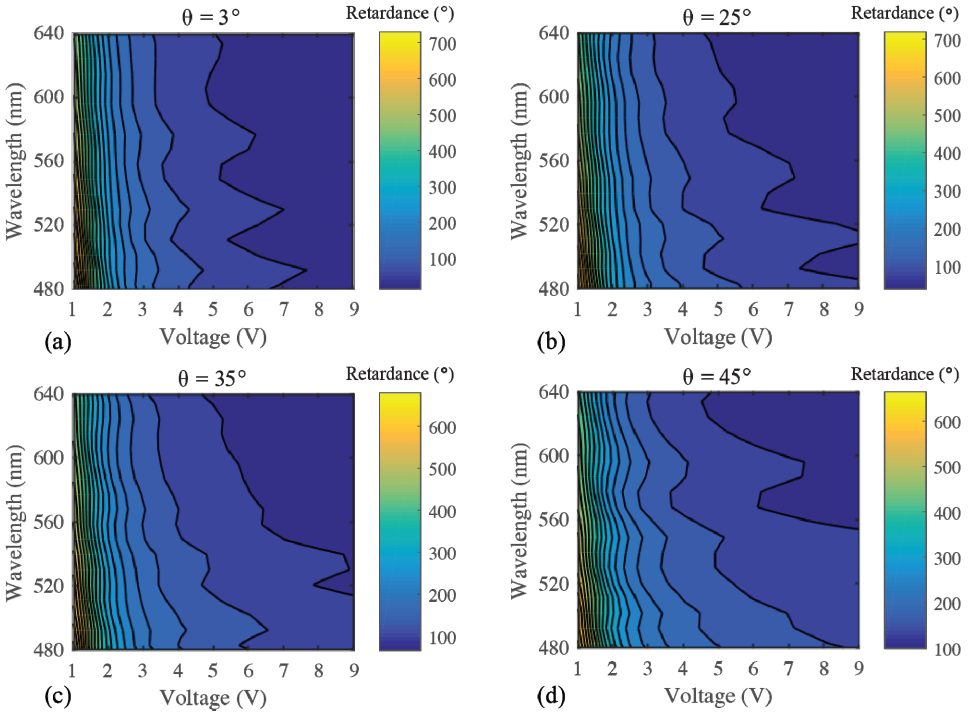

Fig. 3. Retardance measurements obtained in the SF-FDTD simulated experiment for 18 wavelengths and 61 voltages and the incidence angles: (a) 3°, (b) 25°, (c) 35°, and (d) 45°.

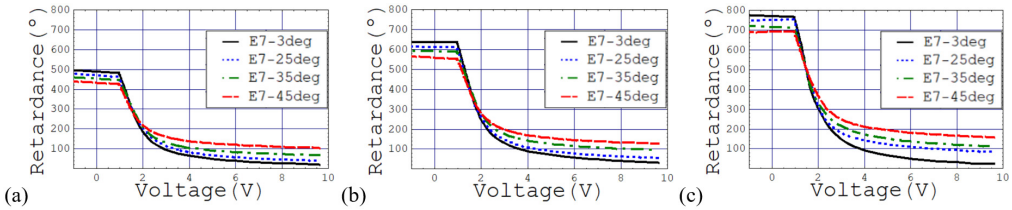

Fig. 4. Retardance simulated measurements for the various incidence angles (in the legend) and for the wavelengths: (a) 633 nm, (b) 532 nm, and (c) 473 nm.

We also produce the values for the situation when no voltage is applied to the device, what it is called the off-state. To this goal we directly consider the results produced by the homogeneous uniaxial anisotropic plate expressions, developed by Yeh and Gu [1, pp. 326-328] or also by Lien [31]. We have already used these expressions in our previous works [14, 17]. In this specific situation, the LC device has a uniform LC director distribution and the exact expression can be used with a higher accuracy. In Table 2 we show the retardance for the 5 angles of incidence and for the three wavelengths for the off-state.

Table 2. Values for the retardance in the off-state.

λ (nm)	Incidence angle (deg)				
	0	3	25	35	45
633	496.4	496.1	476.8	459.6	439.3
532	638.0	637.6	613.1	591.4	565.7
473	776.6	776.2	746.7	720.6	689.7

3. Calibration and discussion

The procedure to obtain the parameters in the model involves fitting the analytical expression to the experimental results. In a first step we fit the off-state parameters, OPD and OPL, using

Optics EXPRESS

the off-state retardance values in Table 2. These off-state parameters are wavelength dependent but do not depend on the angle of incidence. Once obtained, we fit the tilt angle, which depends on the applied voltage. As we did in our initial paper [14] we use the measurements taken at 3° and 35° for calibration of the model parameters, and the other two measurements, at 25° and 45°, to validate and analyze its predictive capability.

3.1. Off-state parameters analysis

We fit the theoretical expression in the model with the retardance measurements to obtain the values for the parameters OPD and OPL when the PA-LC is in the off-state. To serve as a reference, in Table 3 we give the values for OPD and OPL calculated according to the refractive indices and cell gap value in Table 1.

Table 3. True OPD and OPL parameters calculated from the cell gap and the indices of refraction in Table 1.

λ (nm)	633	532	473
OPD(μm)	0.4364	0.4714	0.5102
OPL(μm)	3.0378	3.0578	3.0768

As explained in previous works [14,17], the figure of merit χ^2 to be minimized combines two squared differences: on one hand between theoretical and simulated retardance values normalized by the simulated value, and on the other hand between the theoretical and simulated ratios of the retardance values for the pair of incidence angles considered (3° and 35°) normalized by the simulated ratio. These two normalized squared differences are added up for the three wavelengths. This minimized value for χ^2 is given for each set of fitted parameters in Table 4. The theoretical expressions are nonlinear and to start the iterative optimization process we have to assign initial values to the parameters OPD and OPL. In our previous work [14,17] we remarked that our model provides the same resulting OPD and OPL values for a very wide range of starting values, thus not showing multiple, i.e. ambiguous, solutions. For example, we get the same OPD and OPL values when we apply as initial the values in Table 3 or when we consider initial OPD and OPL as equal to 1 meter: thus, through six orders of magnitude the initial values lead to the same unique result.

As we recently discussed [17], something that we have found when playing against the FDTD data is that the resulting OPD and OPL values depend on the index of refraction considered for the liquid crystal, parameter n_{LC} in Fig. 1. In Table 4 we show the results obtained for OPD and OPL for the three wavelengths and for different values of n_{LC} (first row). We have chosen n_{LC} values ranging from 1.5 to 1.7, which fall within the typical range of values for liquid crystals. Specifically if we take into account the refractive indices for E7 in Table 1, the average refractive index, calculated as $(n_e + 2n_o)/3$, is 1.59, 1.61 and 1.62 respectively for the wavelengths 633, 532 and 473 nm. The average of the three values is 1.61.

Table 4. Fitted OPD and OPL values for different values for n_{LC}, and values for the figures of merit for the off-state χ^2 and for the on-state MSE comparison between theoretical and experimental results.

n_{LC}	1.50	1.60	1.61	1.62	1.65	1.70
χ^2 Off-State	$4.8\text{x}10^{-5}$	$7.1\text{x}10^{-28}$	$2.2\text{x}10^{-18}$	$2.8\text{x}10^{-20}$	$3.7\text{x}10^{-26}$	$2.5\text{x}10^{-20}$
MSE On-State	0.0244	0.0147	0.0141	0.0135	0.0124	0.0124
	(μm)	(μm)	(μm)	(μm)	(μm)	(μm)
OPD(633 nm)	0.4369	0.4364	0.4364	0.4364	0.4364	0.4364
OPL(633 nm)	$24.02\text{x}10^{6}$	6.8456	6.0775	5.4614	4.1772	2.9829
OPD(532 nm)	0.4722	0.4714	0.4714	0.4714	0.4714	0.4714
OPL(532 nm)	$39.89\text{x}10^{6}$	8.5336	7.4609	6.6237	4.9421	3.4506
OPD(473 nm)	0.5113	0.5102	0.5102	0.5102	0.5102	0.5102
OPL(473 nm)	$49.53\text{x}10^{6}$	10.7767	9.2462	8.0910	5.8679	3.9977

Optics EXPRESS

As quality parameters to compare the agreement between theoretical and experimental results for the off-state and for the on-state we show respectively χ^2 (2nd row), already defined, and the mean square difference (MSE) (3rd row). The parameter MSE corresponds to the square difference at each voltage between the theoretical and simulated retardance values normalized by the simulated value. These squared values are added up for the whole range of voltages and for both incidences at 3° and 35°, and then divided by the total number of samples to produce a mean value. The on-state results will be shown in the next Section. We note that only in the case of n_{LC} = 1.50 the figures of merit are clearly worse, but in the rest of the cases they are very similar, with the best MSE for refractive index 1.65 and 1.70, and best χ^2 for refractive index 1.60 and 1.65. If we take a look at the OPD values for the three wavelengths, we see that they are similar to the four decimal number with respect to the ones shown in Table 3, except for n_{LC} = 1.50 where it is similar to the third decimal number, which is still a very good agreement. In the case of OPL, its values are different for all the n_{LC}, diminishing as we increase n_{LC}. They do not coincide with the OPL values in Table 3 even though they are in the same order of magnitude, except for n_{LC} = 1.50. Further analysis on OPL is done in Section 4.2. We conclude that the OPD parameter is physically meaningful and it does not depend on the value considered for n_{LC}, thus it is very robust. Intuitively, since the magnitude we calculate with the model is the retardance, then OPD, which includes the birefringence, must have a much stronger impact than OPL on the fitted retardance result. If we knew the value for the cell gap by some other means, then our model is able to provide reliable birefringence values as a function of wavelength.

Now, we want to compare the results for the MSE in Table 4 with the ones that we presented in Table 5 in our previous paper [17] for the sine-like profile. We note that for the sine-like profile MSE obtained was about 0.0005 whereas for the realistic profiles is about 0.012, i.e. two orders of magnitude worse. As we will see in next Section, this is because in the present paper we consider highly non-linear tilt angle profiles, at which the simplified model loses accuracy.

3.2. On-state parameters analysis

The only on-state parameter is the tilt angle $\alpha(V)$, in Eq. (2). To apply the expression in Eq. (1) we consider the off-state solution in Table 4 for OPD and OPL obtained when n_{LC} = 1.65. The same figure of merit χ^2 is now used for the on-state fitting procedure, and the optimization is run voltage by voltage independently. The experimental values applied correspond to the voltage dependent retardance SF-FDTD values for incidence angles at 3° and 35°. In Fig. 5(a) and 5(b) we show the retardance versus voltage plots for the theoretical fitting using the model (continuous line) and the experimental SF-FDTD data (dots) respectively for the incidence angles at 3° and 35°, and for the three wavelengths. We note that theoretical and SF-FDTD results agree very well with each other at both incidences and also for the three wavelengths.

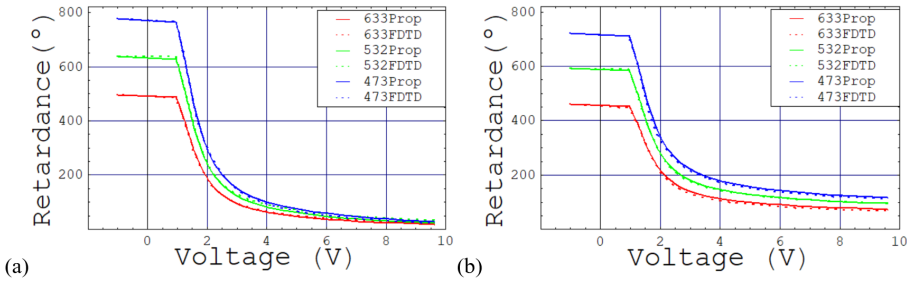

Fig. 5. SF-FDTD experiment (dots) and theoretical fitting with the proposed simplified model (continuous line) for the wavelengths 633, 532 and 473 nm and for incidence at: (a) 3°; (b) 35°.

Optics EXPRESS

In Fig. 6 we show the tilt angle versus voltage obtained from the on-state fitting in Fig. 5 with the proposed simplified model, labeled as "Proposed Model", and the "Average Tilt" corresponding to the mean tilt value across the cell gap for the realistic tilt profiles, shown in Fig. 2. We also plot the difference between these two curves ("Average" minus "Proposed"), that we call "Tilt Difference" in the legend. The tilt difference before 2.2 V is about −5° and after 2.2 V increases to about + 5° and stays almost constant around this value from 4 V till the end. The fitted angle associated with the proposed simplified model can be thought as the tilt angle for an equivalent homogeneous PA-LC layer providing the same retardance as the one given by the non-homogeneous realistic profiles. We see that this equivalent homogeneous tilt is about ± 5° when compared with the average tilt. Thus, we might think of the fitted model angle as a corrected average tilt able to provide correct values for the retardance of the non-homogeneous realistic profiles. If we now look at the "Proposed Model" curve we observe that the monotonic increase of the tilt angle with the voltage shows a highly nonlinear variation with a steep increase before ~2.5 V and a saturation behavior after this voltage. If we look at the retardance curves in Fig. 4 we see that most of the retardance variation occurs before 2.5 V. If we look at the results presented in Fig. 4 in our previous paper [14], the tilt angle range associated with a commercial PA-LCoS device was between 0°-50°, which corresponds to a maximum voltage of ~2V in Fig. 6, thus avoiding the saturation regime. This is actually the tilt angle range simulated in [17] using the sine-like profile. Since there is no saturation in the realistic profile curve within this voltage range, the profile can be reasonably approximated by a sine-like profile as done in [17].

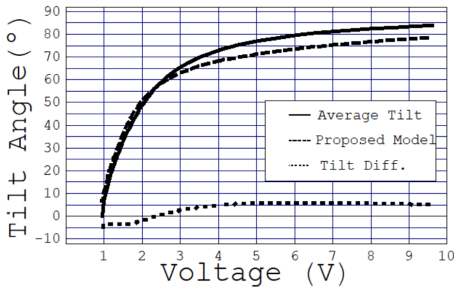

Fig. 6. Tilt angle as a function of voltage.

To make more visible the accuracy of the proposed model we use the results in Fig. 5 and calculate the difference between the theoretical and the FDTD-experimental retardance values normalized by the theoretical ones. In Figs. 7(a) and 7(b) we show, respectively for incidence at 3° and 35°, this normalized retardance difference for the three wavelengths. Deviation is very small, less than ± 0.05 (i.e. ± 5%,) for voltages smaller than 2.5 V: that is, deviation only becomes larger for such tilt angles as 60° and above. We see that deviations are larger for quasi-normal incidence at 3° when compared with incidence at 35°: in the latter deviation never exceeds ± 10%.

Optics EXPRESS

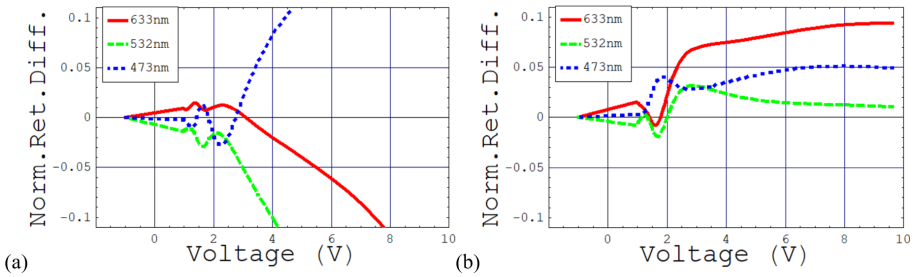

Fig. 7. Difference between theoretical and SF-FDTD-experimental retardance normalized by the theoretical value for wavelengths 633, 532 and 473 nm and for incidence at: (a) 3°, and (b) 35°.

Now, using the fitted tilt angle in Fig. 6 we test the predictive capability of the model: we calculate the retardances at the other two incidence angles. In Figs. 8(a) and 8(b), respectively for incidence at 25° and 45°, we show both the theoretical values calculated with the model (continuous line) and the SF-FDTD experimental values (dots). Retardance values are plotted as a function of the model-fitted tilt angle instead of the applied voltage. Remember that tilt angle 60° is associated with an applied voltage of 2.5 V, where the saturation regime of the tilt angle versus voltage starts (Fig. 6). When representing retardance versus tilt angle the curve becomes smoother than in Fig. 5, where X-axis corresponds to applied voltage. We note the good agreement between model and SF-FDTD experiment.

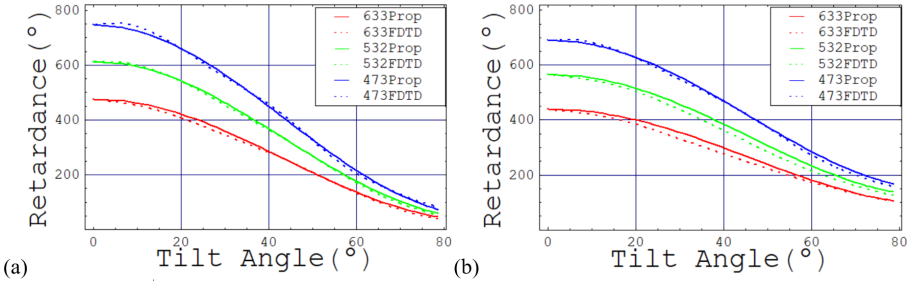

Fig. 8. SF-FDTD experiment (dots) and prediction with the proposed simplified model (continuous line) for the wavelengths 633, 532 and 473 nm and for incidence at: (a) 25°; (b) 45°.

Once again, to assess the predictive capability is more useful to represent the normalized retardance difference as we did in Fig. 7. This is done respectively for incidence at 25° and 45° in Figs. 9(a) and 9(b). We see that the model proposed predicts the retardance with relative uncertainties that in most of the tilt angle range is about 5% or less. In the case of incidence at 45° and for the red wavelength this range is exceeded to 7% at about 40° tilt angle but then after 60° it becomes smaller than 5%. In general, both from Figs. 7 and 9, deviations become larger at very large tilt angles (larger than 60°). We see from the results in this Section that when the tilt angle profile is highly non-linear, including saturation plateaus, the simplified model shows larger deviation. In [14], experimental data, and in [17], sine-like computed profile, it is clear that we are not in this highly non-linear regime and accuracy of the model stayed within 5%.

Optics EXPRESS

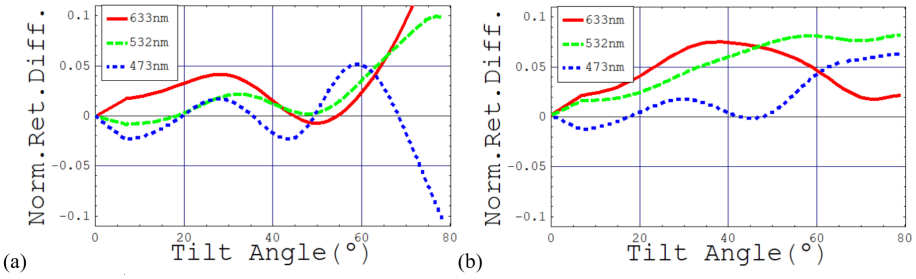

Fig. 9. Difference between predicted and SF-FDTD experimental retardance normalized by the predicted value for wavelengths 633, 532 and 473 nm and for incidence at: (a) 25°, and (b) 45°.

3.3. Non-homogeneous sine profile approximation

In the following, we use the realistic tilt profiles to fully exploit the possibilities of the proposed simplified model. In most of phenomena, availability of analytical expressions [18] usually eases the mathematics and it also provides deeper physical insight. In principle, when applied voltages are smaller than the ones producing a saturation in the tilt angle, the sine tilt profile might work as a good first approximation to the more complex nonlinear tilt angle profiles across the LC cell thickness. Actually, in [16,17] we considered sine-like profiles for the tilt angle as a function of the applied voltage. From the derivation in the present Section we can conclude within which limits this is actually a good approximation to the functioning of PA-LC devices. At the end of this Section we will apply these results to fit the experimental data in [14] to its equivalent sine-like tilt angle profile.

In the sine profile, the tilt angle $\alpha_{\sin}$ across the cell thickness z varies as

$$\alpha_{\sin} = \alpha_{\max} \sin(\pi z / d), \tag{3}$$

where d is the cell gap, and $\alpha_{\max}$ is the maximum tilt angle, which occurs in the midlayer of the cell. For numerical calculations, the LC cell can be considered as decomposed into a large number of sublayers so that within each of them the tilt angle is constant. Using the model, from Eq. (1), the contribution $\Delta\Gamma$ to the retardance from a sublayer of thickness Δz is

$$\Delta\Gamma = \frac{2\pi}{\lambda}\frac{(OPL/d)}{\cos\theta_{LC}}\left(\frac{1+(OPD/OPL)}{1+(OPD/OPL)\cos^2\phi}-1\right)\Delta z. \tag{4}$$

What we propose is to fit the nonlinear sine profile to the equivalent homogeneous tilt providing the same retardance. Both for the nonlinear sine profile and for the homogeneous tilt we apply the proposed simplified model and we use the OPD and OPL calibration obtained previously for $n_{LC} = 1.65$. The total retardance is given by the addition of the forward and backward paths, which in the case of a homogeneous tilt α_{hom} and taking into account Eqs. (1) and (2) is given by

$$\Gamma_{total}^{\text{hom}}(\theta_{inc},\alpha_{\text{hom}}) = \frac{2\pi}{\lambda}\left(\frac{OPL}{\cos\theta_{LC}(\theta_{inc})}\left[\frac{1+(OPD/OPL)}{1+(OPD/OPL)\cos^2\phi(\theta_{inc},\alpha_{\text{hom}})}+\frac{1+(OPD/OPL)}{1+(OPD/OPL)\cos^2\phi(-\theta_{inc},\alpha_{\text{hom}})}-2\right]\right). \tag{5}$$

Let us substitute the layer thickness by its normalized parameter z/d = z'. Then Eq. (3) becomes $\alpha_{\sin} = \alpha_{\max}\sin(\pi z')$ and the integration of the sublayers, described in Eq. (4), with the sine profile is described by

Optics EXPRESS

$$\Gamma_{total}^{\sin}\left(\theta_{inc},\alpha_{\max}\right)=\frac{2\pi}{\lambda}\frac{OPL}{\cos\theta_{LC}\left(\theta_{inc}\right)}\cdots \\ \cdots\int_0^1\left(\frac{1+\left(OPD/OPL\right)}{1+\left(OPD/OPL\right)\cos^2\phi\left(\theta_{inc},\alpha_{\sin}\left(\alpha_{\max},z'\right)\right)}+\frac{1+\left(OPD/OPL\right)}{1+\left(OPD/OPL\right)\cos^2\phi\left(-\theta_{inc},\alpha_{\sin}\left(\alpha_{\max},z'\right)\right)}-2\right)dz', \tag{6}$$

where we observe that the result does not depend on the cell thickness *d*. We give values to the $\alpha_{\max}$ and for each of the values we solve numerically the equation

$$\Gamma_{total}^{\sin}\left(\theta_{inc},\alpha_{\max}\right)=\Gamma_{total}^{\hom}\left(\theta_{inc},\alpha_{\hom}\right), \tag{7}$$

where the only unknown parameter is the tilt angle $\alpha_{\hom}$ for the equivalent homogenous slab, and we obtain the relation $\alpha_{\hom}=\alpha_{\hom}\left(\alpha_{\max}\right)$. In Fig. 10(a) we plot the inverse of this relation, where we see that for a maximum $\alpha_{\max}$ value of 90° the corresponding homogeneous equivalent tilt angle is about 55°. The curve in Fig. 10(a) is obtained substituting OPD and OPL values for the red wavelength and at incidence $\theta_{inc}=45^{\circ}$. We have applied the same procedure at other wavelengths, i.e. using other OPD and OPL values from Table 4, and for other angles of incidence θ_{inc} and the resulting relations $\alpha_{\hom}=\alpha_{\hom}\left(\alpha_{\max}\right)$ are the same with deviations smaller than ± 1° between them. Thus, we can consider that it is basically invariant to the wavelength and to the angle of incidence. If we combine $\alpha_{\hom}=\alpha_{\hom}\left(\alpha_{\max}\right)$ with the fitted tilt versus voltage in Fig. 6, then we obtain the relation $\alpha_{\max}=\alpha_{\max}\left(V\right)$ for the specific LC cell simulated in the paper. We show this relation in Fig. 10(b), where we see that the sine profile fit is only valid for voltage values smaller than 2.2 V, since for larger voltage values the $\alpha_{\max}$ parameter becomes larger than 90°, which is not possible.

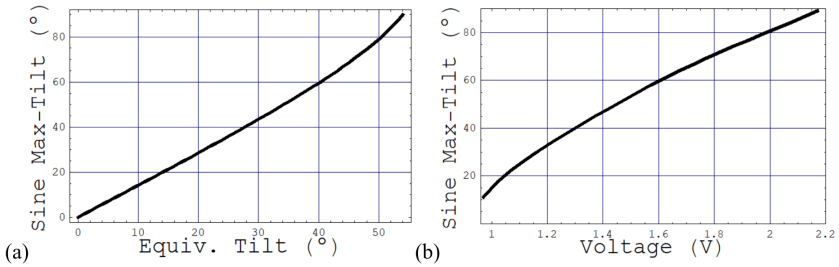

Fig. 10. Relation for $\alpha_{\max}$ (sine profile), (a) vs. tilt angle of an equivalent homogenous slab and, (b) vs. voltage.

In Fig. 11 we compare for some voltage values the realistic and the sine tilt profiles. Let us remind that the realistic tilt profile involves the numerical solution of complex equations where the knowledge of the specific values for a number of LC material and cell parameters must be known in advance. To obtain the equivalent sine profile providing the same retardance this is not necessary, as we have just shown. In Fig. 11 we see that as the voltage increases the realistic profile loses its sine-like features. However, the retardance provided by both curves is still the same for any angle of incidence within 0°-45° and for any wavelength in the visible. In the case when an approximation to the nonlinear tilt profile is necessary, then the procedure just described to obtain the best-fitted sine-like profile is a very efficient approach. For the specific cell simulated in this work, the voltage range from 0 to 2.2 V covers a very significant amount of the retardance dynamic range, as we have seen in Fig. 4.

Optics EXPRESS

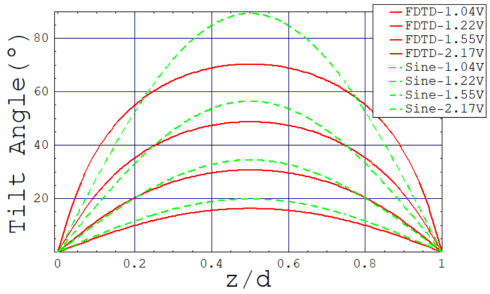

Fig. 11. Comparison between the realistic and the sine tilt profiles for a series of voltages.

The analysis in this Section helps to understand that the application of analytical sine-like profiles for the tilt angle in previous works [16,17] is a good approximation to the functioning of commercial PA-LC devices where the equivalent tilt angle is within the range 0°-50°, as we saw in [14], thus avoiding the saturation regime. As an application of this sine tilt angle profile fitting procedure to a real device, we will apply it to the experimental measurements obtained for the commercial PA-LCoS in [14]. The calibrated values for its parameters obtained in this paper are shown in Table 5, OPD and OPL, and in Fig. 12, tilt angle versus gray level (gray level is related to the applied voltage). We substitute in Eq. (7) the OPD and OPL values for the red wavelength and we consider and angle of incidence θ_{inc} of 45°. Substituting other values for OPD, OPL and θ_{inc} produce deviations smaller than ± 1° in the fitted curve $\alpha_{\text{hom}} = \alpha_{\text{hom}}(\alpha_{\max})$, i.e. not significant. In Fig. 13(a) we plot the inverse of this curve, i.e. $\alpha_{\max} = \alpha_{\max}(\alpha_{\text{hom}})$, and from the combination of the two previous plots we obtain in Fig. 13(b) the curve $\alpha_{\max} = \alpha_{\max}(gray)$.

Table 5. OPD and OPL parameters obtained for the commercial PA-LCoS in [14].

λ (nm)	633	532	473
OPD(μm)	0.528	0.594	0.649
OPL(μm)	2.576	2.606	6.893

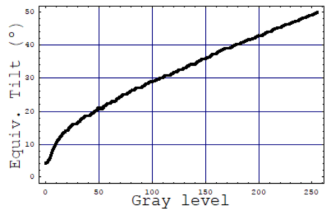

Fig. 12. Tilt angle as a function of gray level for the commercial PA-LCoS in [14].

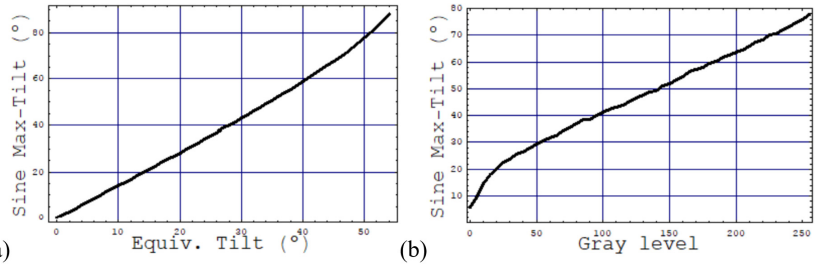

(a) (b)

Fig. 13. From the experimental data for the commercial PA-LCoS in [14]. Relation between $\alpha_{\max}$ (sine profile), (a) vs. tilt angle of an equivalent homogenous slab and, (b) vs. gray level (applied voltage).

Optics EXPRESS

In Fig. 14 we show the resultant tilt angle profiles at some selected gray levels, where we see how the midlayer tilt angle increases with the increase in gray level. We also see that for the maximum gray level, the midlayer tilt angle is still smaller than 80°, thus the sine-like profile is a good approximation to the realistic tilt angle profile.

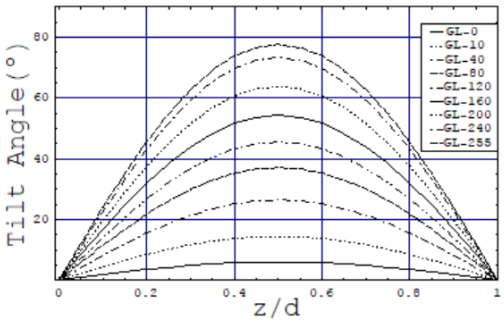

Fig. 14. Sine tilt profiles as a function of the gray level.

4. Applications of the physical simplified model

4.1. Spectral and angular retardation

As demonstrated, our model is able to produce accurate values of the retardance with uncertainties smaller than 5%, especially within the range of applied voltages in commercial devices. Using the SF-FDTD realistic retardances let us explore the accuracy when calculating spectral retardance across the whole visible spectrum and for a series of incidence angles ranging from 0° to 45°. This is important if we plan to use the model for spectral retardance control in applications such as the one reported by Moreno et al. [32], where they show a system that acts as an optical retarder where the retardance spectral characteristics can be defined at will, and it can be reprogrammed in real time.

For the PA-LC described in the SF-FDTD simulation, in Fig. 15 we show the comparative of the retardance across the whole visible spectrum calculated with the proposed simplified model and the SF-FDTD computed experimental data. We show this comparative at three different incidence angles (see legend), and for the minimum and maximum applied voltage, respectively in Figs. 15(a) and 15(b). For the minimum applied voltage (maximum retardance values) the agreement across the visible is very good for both the model and the SF-FDTD values. In the latter, we appreciate some oscillations which are probably due to the residual interference effects not eliminated by the antireflection (AR) coating considered in the SF-FDTD calculation. We see that the change in retardance across the whole visible spectrum is larger than 200° for any incidence angle. In Fig. 15(b), for the maximum applied voltage (minimum retardance) the agreement between model and SF-FDTD experimental data is also good and we also see the oscillations in the SF-FDTD values. Now the change in retardance across the whole visible spectrum is much smaller than in plot (a), especially when inciding at 0° (normal incidence) where the change in retardance is about 10°. Choosing the appropriate voltage values we could design specific spectral retardance curves as it was done by Moreno et al. [32] but now from a more physical and analytical perspective.

Optics EXPRESS

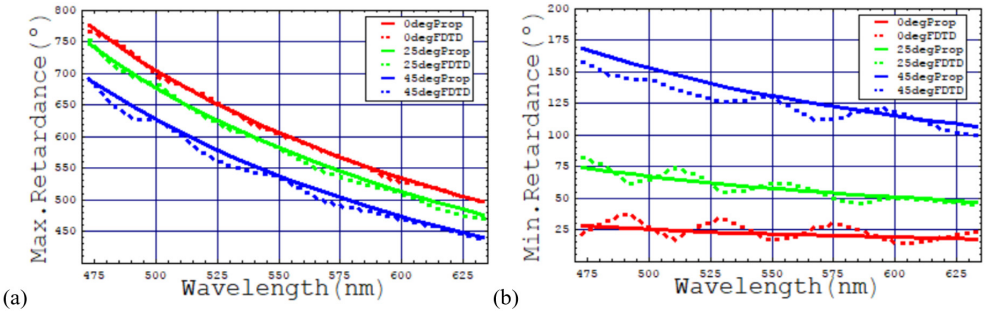

Fig. 15. Proposed simplified model (continuous line) and SF-FDTD experimental (dots) retardance versus wavelength and for three incidences. (a) Maximum and (b) minimum retardance values.

In Fig. 16 we plot the retardance dynamic range for each of the wavelengths across the visible spectrum and for the three incidence angles. This is done by subtracting the maximum and minimum retardance spectral curves in Figs. 15(a) and 15(b). This is useful if we plan to use the PA-LC device for phase-only applications, where we usually need a 360° phase-shift dynamic range. In Fig. 16 we see that our simulated PA-LC device is able to provide the required 360° phase-shift dynamic range for any wavelength in the visible and for incidences at 0° and 25°. At 45° incidence angle, the range is larger than 360° for wavelengths smaller than 575 nm. Once again, we see that the agreement between the predictions with our simplified model and the SF-FDTD values is very good.

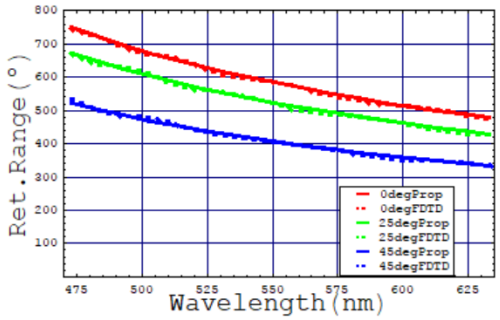

Fig. 16. Retardance dynamic range. Proposed simplified model (continuous line) and SF-FDTD experimental (dots) retardance versus wavelength and for three incidences.

4.2. Analytical design of PA-LC devices

When we compared in Section 3.1 the fitted OPD and OPL values (Table 4) with their true values (Table 3) we found out that OPD converged into its true value. However, OPL was clearly different from its true value and it varied with n_{LC}. The question now is to which extent deviations in OPL actually affect the resultant retardance calculated value. In the following, as refractive index for LC E7 we consider its average value $n_{LC} = 1.61$, discussed in relation with Table 4. If we substitute the true OPD and OPL values in the expression for the off-state figure of merit we obtain $\chi^2 = 0.0008$. Furthermore, if the true OPD and OPL values are used in the on-state optimization, the value obtained for the on-state figure of merit is MSE = 0.012. In principle, the χ^2 off-state figure of merit has worsen with respect to the optimized OPL value expressed in Table 4, however it is still a very good value. For the on-state MSE figure of merit, the value obtained is very similar to the other ones expressed in Table 4. Therefore, in principle we find that using the true OPL value instead of the fitted one is not affecting the predictive capability of the simplified model. This opens a new range of applications to the simplified model: it can be used to calculate the performance of PA-LC

Optics EXPRESS

cells as a function of the LC compound and the cell gap. It is then an alternative to more complex, sophisticated and computing intensive approaches [1–3,15].

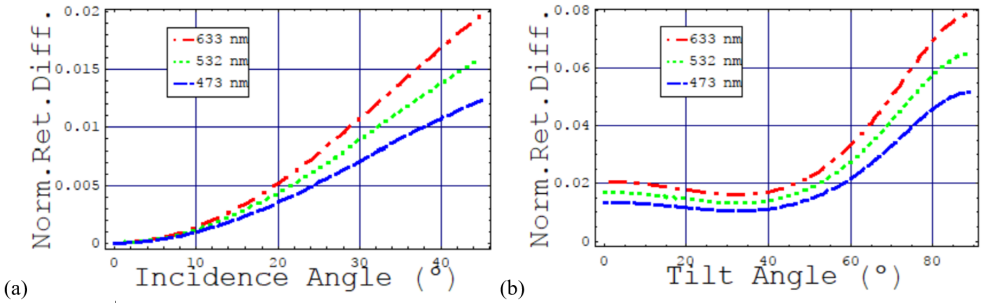

Fig. 17. With the simplified model, usage of the true OPL to calculate the retardance. Normalized retardance difference in the: (a) Off-state, against the true off-state retardance, and (b) On-state, for an angle of incidence of 45°, against the calculation using the fitted OPL.

To learn about the level of uncertainty produced by the simplified model when applying the true OPD and OPL values, let us compare its results against the exact ones provided by, in principle, more accurate and complex approaches. We consider the same PA-LC cell with nematic LC E7 and cell gap of 2 µm. In Fig. 17(a) we show this comparison in the off-state. We represent the difference between the exact off-state retardance values in Table 2 and the ones from the simplified model using the true OPD and OPL values, normalized by the exact retardances. This is done for the three wavelengths and as a function of the incidence angle. We see that deviation from the exact value increases with the angle of incidence. In any case it is smaller than 2%. A different representation is established for the on-state, i.e. as a function of the tilt angle, in Fig. 17(b). Now the comparison is between the retardance calculated with the simplified model applying respectively the fitted and the true OPL values, and normalized by the retardance using the fitted OPL. In both cases OPD value is the same since, as already shown, the fitted value is equal to the true one. This normalized retardance difference is shown at an angle of incidence of 45°. We see that differences increase with the tilt angle reaching values close to 8%. However, in the range of tilt angle found in commercial devices, from 0 to about 50°, deviation is smaller than 4%, which is accurate enough for most of the applications.

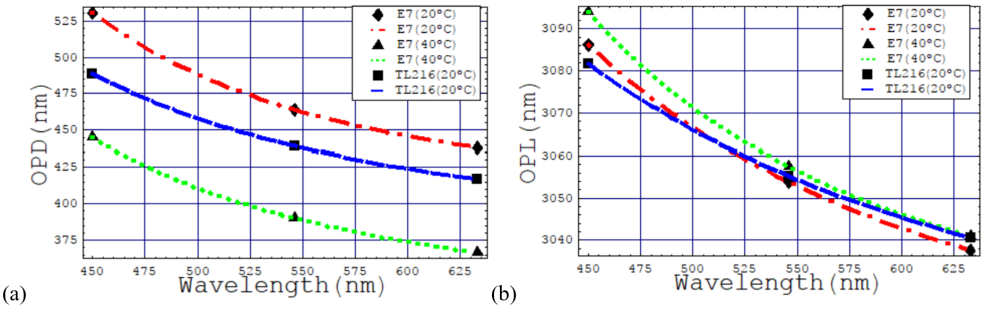

Fig. 18. Values for OPD, in (a), and OPL, in (b), for two LC compounds and two temperatures, for a cell gap of 2 µm. Data points in the plots are the sample values use to fit the extended Cauchy relation across the visible.

We have checked that the true OPL provides satisfactory retardance calculations with the simplified model. Therefore, a novel area of application of the simplified model arises: it is not only a reverse-engineering model useful to calibrate and predict the retardance of commercial devices, but it is also useful as a direct model to calculate which results can be expected in the construction of PA-LC cells. This means that, when choosing the LC

Optics EXPRESS

compound and the cell gap, it can be used to design these PA-LC cells. As an example of application, in Fig. 18(a) and 18(b) we show respectively the OPD and OPL values as a function of wavelength for two different LC mixtures, E7 and TL-216. The latter, TL-216, is a high birefringence LC mixture used in color-sequential liquid-crystal-on-silicon (LCoS) projection displays. In the case of E7 we show the values at temperature 20°C, used in the SF-FDTD calculations in the paper, and at 40°C. These OPD and OPL values are calculated from the tabulated data for the ordinary n_o and the extraordinary n_e refractive index given in the paper by Li et al. [24] and for a cell gap of 2 μm. We use the tabulated data at three wavelengths (points in the plots) to fit the extended Cauchy relation (curves in the plots) across the visible spectrum.

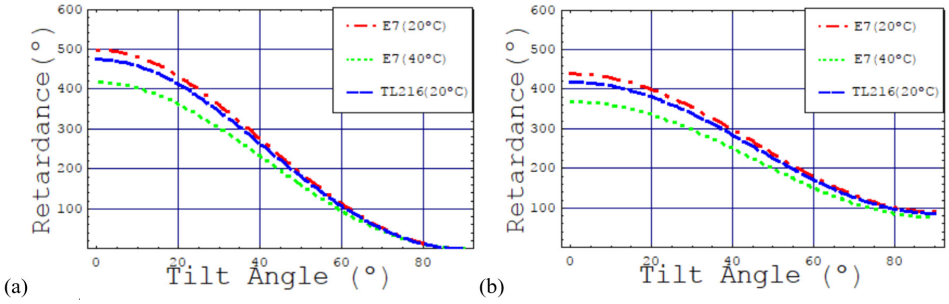

Fig. 19. Using the proposed simplified model, simulated retardance at 633 nm, at incidence angles: (a) 0°; (b) 45°.

From the extended Cauchy relations in Fig. 18 and using Eqs. (1) and (2) for the simplified model, we calculate the retardance as a function of the tilt angle, i.e. on-state. In Fig. 19(a) and (b) we show the results for the wavelength 633 nm respectively for incidence at 0° and 45°, and in Figs. 20(a) and 20(b) for 473 nm, also for incidence at 0° and 45°. These kind of calculations, with an expected uncertainty of less than 4% for tilt angles smaller than 50°, enable to anticipate temperature, incidence angle, spectral and applied voltage dependence of the retardance. This might prove very helpful approach, very fast and easy to use in the design of PA-LC devices.

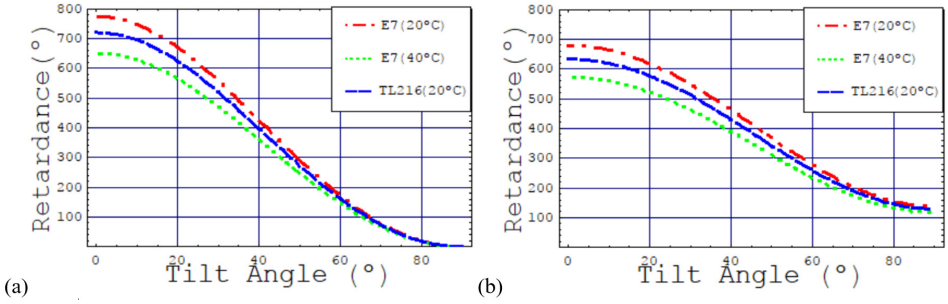

Fig. 20. Using the proposed simplified model, simulated retardance at 473 nm, at incidence angles: (a) 0°; (b) 45°.

5. Conclusions

The construction of a virtual PA-LC cell has been a useful approach to obtain a deeper insight into the physical significance of the parameters of the PA-LC model recently proposed. We have applied the values for the physical parameters of the E7 LC compound and for a cell gap of 2 μm. Realistic non-linear tilt profiles and application of efficient SF-FDTD methodology has produced experimentally-like retardance values. We have obtained that two of the three parameters, the OPD and the tilt angle, are physically meaningful and are useful to probe into internal characteristics of the PA-LC devices. We have also demonstrated an efficient

Optics EXPRESS

reverse-engineering approach to calculate the sine-like equivalent tilt profile, which is a useful approximation for the non-linear tilt angle across the cell as a function of the applied voltage. The model shows a high degree of predictive capability, what makes it very useful to characterize the possibilities of PA-LC devices in novel applications such as in the experiments dealing with unconventional polarization states [33,34]. In addition, we have demonstrated the versatility and applicability of the model for spectral and angular retardation calculations. We have also shown how the model has the potential to simulate the retardance for novel PA-LC devices as a function of the LC compound and cell gap. Therefore, it is not only a reverse-engineering model but it also constitutes an analytical alternative to the usual numerical approaches for PA-LC devices design and construction.

Funding

Ministerio de Economía, Industria y Competitividad (Spain) under projects FIS2017-82919-R (MINECO/AEI/FEDER, UE) and FIS2015-66570-P (MINECO/FEDER), and by Generalitat Valenciana (Spain) under project PROMETEO II/2015/015.